NUCL SCI TECH (2017) 28:25
DOI 10.1007/s41365-016-0177-4

Alignment calibration and performance study of the STAR PXL detector

Long Ma[1,2] · Xin Dong[3] · Hao Qiu[4] · Spiros Margetis[5] · Yu-Gang Ma[1,6]

Received: 3 October 2016 / Revised: 14 November 2016 / Accepted: 16 November 2016 / Published online: 28 December 2016

Abstract We report in this paper the alignment calibration of the STAR pixel detector (PXL) prototype for the RHIC 2013 run and performance study of the full PXL detector installed and commissioned in the RHIC 2014 run. PXL detector is the innermost two silicon layers of the STAR heavy flavor tracker aiming at high-precision reconstruction of secondary decay vertex of heavy flavor particles. To achieve the physics goals, the calibration work was done on the detector with high precision. A histogram-based method was successfully applied for the alignment calibration, and the detector efficiency after alignment was studied using both $p+p$ collision data and cosmic ray data.

Keywords Alignment calibration · Heavy flavor tracker · STAR

This work was supported in part by the National Natural Science Foundation of China (No. 11421505) and the Major State Basic Research Development Program in China (No. 2014CB845400).

✉ Yu-Gang Ma
ygma@sinap.ac.cn

1 Shanghai Institute of Applied Physics, Chinese Academy of Sciences, Shanghai 201800, China

2 University of Chinese Academy of Sciences, Beijing 100049, China

3 Nuclear Science Division, Lawrence Berkeley National Laboratory, Berkeley, CA 94720, USA

4 Purdue University, West Lafayette, IN 47907, USA

5 Kent State University, Kent, OH 44242, USA

6 ShanghaiTech University, Shanghai 200031, China

1 Introduction

The study of high-energy heavy-ion collisions at RHIC gives insights into the exploration of the strongly interacting quark–gluon plasma (QGP) and QCD phase transition [1–4]. Investigation of particles produced during the initial phase of the collision where hard interactions of partons occur is proposed as sensitive probe of the state of matter [5, 6]. Theoretically, due to much larger mass than light quarks, heavy quarks are expected to thermalize more slowly than light quarks. Heavy quarks produced at the early stages of the collision fully experienced the evolution of the QGP matter and are sensitive to the medium characteristics. The nuclear modification factor of heavy quarks can be used to study their energy loss mechanisms inside the QGP matter. And heavy quark flow is proposed to be a good indicator of collective motion which can be experimentally measured through the flow measurement of their final hadronized particles [5]. All the above features make heavy quark an ideal probe for QGP matter properties in high-energy heavy-ion collisions [7, 8].

However, due to a low abundance of produced heavy quarks and large multiplicity environment in heavy-ion collisions, measurements of open heavy flavor particles from hadronic reconstruction are experimentally very challenging without secondary vertex reconstruction [9]. A precision vertex detector is required as an important tool to access heavy flavor physics study. Heavy flavor tracker (HFT) in the STAR experiment at RHIC was primarily designed to study heavy flavor particles through direct topological reconstruction of displaced vertices with greatly reduced combinatorial background [10].

With the precision tracking resolution, the HFT detector enables topological reconstruction of heavy flavor particle decays and separates them from the event collision vertices. Its anticipated performance has been studied by simulation work [11]. There are many important topics that can be studied with HFT. For example, charm triggered correlations which characterize the charm quark energy loss inside the medium and Λ_c/D^0 ratio for testing the coalescence model. The B meson and bottom quark yields can also be measured with the HFT, for example, through B decaying to J/Ψ or single leptons [6].

In the RHIC 2013 run, a PXL prototype with three sectors was installed in the STAR experiment. Low-luminosity $p+p$ collision data were taken during the engineering run for testing purpose. The full HFT detector was installed and commissioned since early 2014 in the RHIC 2014 run. To fully exploit the high resolution of PXL detector and performance of the whole HFT, it is essential to calibrate the geometrical placement of the different elements with high precision. With this in mind, alignment procedures were developed to refine the geometries during commissioning. In this paper, we report the alignment calibration for the sub-sector of the HFT PXL detector in STAR TPC global coordinate and performance study of the full PXL detector. Detector performance was also studied and monitored during the operation of the HFT system during 2014 RHIC run.

2 Experimental setup

In the STAR experiment, the main tracking system is the time projection chamber (TPC), the time-of-flight (TOF) detector and barrel electromagnetic calorimeter (BEMC) [9, 12–14]. The TPC is the main tracking system which provides complete tracking for charged particles [15]. The TPC is along the beam line with full azimuth coverage and a pseudo-rapidity range of $|\eta| \leq 1$. The full TPC detector is composed by 24 super-sectors with 12 at each end. Charged particle track momentum is determined based on the track curvature in the detector in a 0.5 Tesla magnetic field [9, 12, 13].

To improve STAR tracking capability enabling for precision study of heavy flavor particles, a novel detector—heavy flavor tracker (HFT)—is designed and installed in STAR. HFT is the innermost part of STAR and consists of 3 sub-detectors with active elements at 2.8 to 22 cm radially from the center of the beam pipe: silicon strip detector (SSD), intermediate silicon tracker (IST) and silicon pixel (PXL) detector. Figure 1 shows the schematic beam-eye view of the HFT detector. The two outermost layers are silicon strip detectors located at a radius of 22 cm from the beam axis and composed of double-sided silicon strip modules with 95 μm pitch. From the outside in, the second

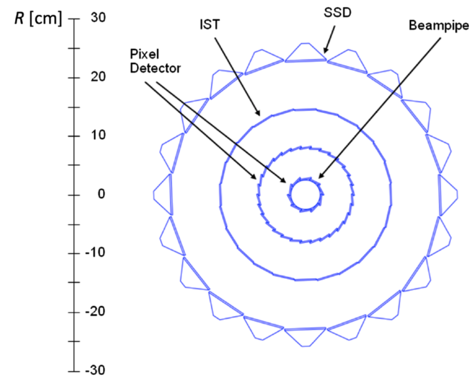

Fig. 1 (Color online) Schematic beam-eye view of the STAR heavy flavor tracker

layer is the intermediate silicon tracker (IST), a layer of single-sided strips. IST guides tracks from the SSD through the innermost PXL detector. It is composed of 24 liquid-cooled ladders equipped with 6 silicon strip-pad sensors—single-sided double-metal silicon pad sensors with 600 μm × 6 mm pitch. IST is located at a radius around 14 cm with thickness less than 1.5% radiation length. The SSD and IST can also help to reduce pileup tracks because they are fast detectors in contrast to the TPC.

The two innermost layers are PXL detectors made from state-of-the-art ultra-thin CMOS monolithic active pixel sensors (MAPS) with 20.7 μm × 20.7 μm pitch and thinned down to 50 μm, delivering ultimate pointing resolution that allows for direct topological identification of heavy flavors [5, 16]. This is the first time that MAPS technology is used in a collider experiment based on the CMOS technology. The full pixel detector has 10 sectors grouped into 2 halves mounted on a supporting tube with 3 kinematic mounts. Each sector is composed of 4 ladders: 3 ladders at the outer layer and 1 ladder at the inner layer, and is located at 8.0 cm (inner) and 2.8 cm (outer) from the center, respectively. The full detector consists of 400 sensors in total. For each sensor, 928 × 960 pixels are distributed on the 2 cm × 2 cm sensor with 20.7 μm pitch. The goal of the PXL detector is to measure the track pointing resolution with high accuracy enabling high-precision secondary decay vertex reconstruction.

In the RHIC 2013 run, three PXL sectors in separated spatial azimuth angles with full supporting mounts were successfully installed into the STAR detector as the HFT PXL detector prototype. All three sectors were surveyed in a workshop with machine measurement before installation. Global alignment calibration was done using $p+p$ collision data. The full HFT system was installed before the RHIC 2014 run, and the detector performance was studied with both zero-field and full-field cosmic ray data. Figure 2 shows the configuration of the PXL half detector and installation in RHIC 2014 run.

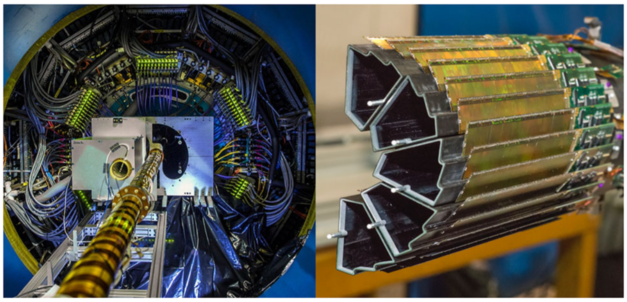

Fig. 2 (Color online) (*Left*) Installation of the STAR heavy flavor tracker. (*Right*) Configuration of the half PXL detector

3 Detector calibration and performance study

Calibration was done for the PXL prototype in the RHIC 2013 HFT engineering run and the 2014 HFT physics run. Low-luminosity $p+p$ collision data and clean cosmic ray data were taken for the alignment and performance studies of the full PXL detector during the run period. The goal of alignment is to obtain correction parameters that can be introduced to refine the geometry of a given element with precision reaching the designed goal. Global alignment of the PXL detector was done with tracking in the TPC global coordinate and association with the hits on PXL layers.

3.1 Alignment calibration of the pixel detector prototype

The HFT PXL detector is designed to offer high hit position resolution at the level of 10 μm. In order to fully exploit the potential of the HFT, the detector geometry needs to be calibrated after installation to determine any deviations from their designed positions. A histogram-based alignment method was developed for HFT alignment with full procedures tested in the 2013 HFT engineering run.

Alignment calibration follows the stream as shown in flowchart in Fig. 3. The procedures follow the steps of first preparing the calibration sample (data in ROOT file format), then getting sector initial geometry information from survey measurements and generating histograms for track-based alignment according to the alignment algorithms (coded with makeHFTPlot.C in the flowchart). By analyzing the histograms, one can extract alignment parameters (coded with HFTDraw.C in the flowchart). The alignment parameters are written back to geometry tables for correction. Several steps need to be finished to go through all the procedures. The final parameters can be fixed after several iterations.

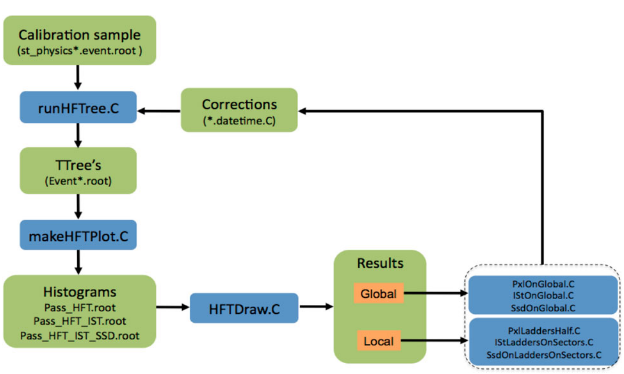

Fig. 3 (Color online) Flowchart showing the procedures of PXL alignment calibration

The geometry tables of the detector are in the form of four-dimensional matrices characterizing the shift and rotation operations at the same time. The alignment correction is done on an individual sector bases by modifying geometry tables in matrices. The full geometry transformation is obtained by multiplying successive matrices. The whole transformation chain is as follow:

$$\begin{aligned} PXLOnGlobal &= TpcGlobal * PxlOnTpc * SectorOnPxl \\ &\quad * (SensorOnSector), \\ SensorOnSector &= LadderOnSector * SensorOnLadder \\ &\quad * PxlSensor. \end{aligned} \tag{1}$$

where *PXLOnGlobal* represents the single pixel geometry position in STAR TPC global coordinate system and *SensorOnSector* represents sensor position in sector coordinate system. The pixel detector alignment below sector level is done using the survey measurement with a coordinate measurement machine as one can see in Fig. 4 showing the PXL sector on metrology stage. Sensor surface deformation due to uncontrollable mechanical effect in sensor production and assembling can be probed by survey measurement. The goal of the survey is to measure within PXL hit error any deviation of each PXL component from their designed position. Sensor survey performs 11×11

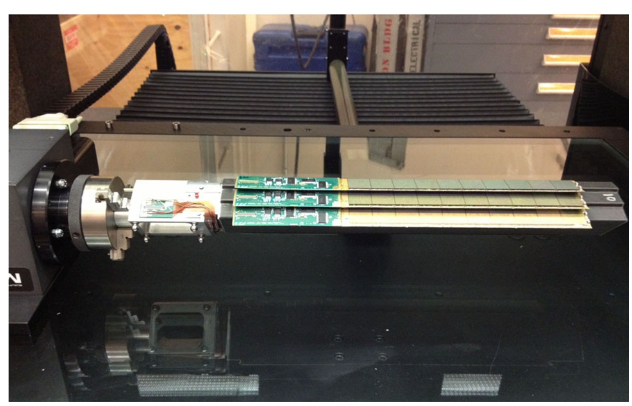

Fig. 4 (Color online) PXL sector on metrology stage for 2013 HFT engineering run

measurements on each chip, with in total more than 5000 steps and around 7.5 h time for each sector. The precision of the machine survey measurement is smaller than 10 μm and is required to be repeatable within 10 μm for individual sensor. Within a chip, the surveyed profile is described by the thin-plate spline (TPS) method, which fills up the whole profile from finite number of measurements. Thin-plate spline method is applied for correcting deviations from an ideal plane for PXL sensors. For individual sub-detector alignment below sector level, the geometry information for individual pixels with respect to each sector is precisely obtained from survey, and these parameters remain unchanged in the track-based alignment.

For PXL detector, the fluctuation of the sensor surface measured in the sensor survey is found to be at the level of ±30 μm, which is larger than the intrinsic pixel detector hit error. Because the uneven surface of the sensors might bring in significant effect on the track–hit residual, we need to measure sensor surface and correct it. As shown in Fig. 5, residual corrections need to be done on single-sensor basis with considering the sensor surface profile obtained from TPS method for track-based alignment.

Starting from survey-based alignment, which obtains the initial geometry information from mechanical survey, track-based alignment, which relies on the TPC track for the PXL alignment, was performed during the data taking of STAR [17, 18]. Sector alignment with regard to the STAR TPC global coordinate system was done. The track-based alignment is on the general idea of minimization of the residuals between the track projection and the hit positions of all detectors starting from initial survey. The residual is defined as the distance between the intersection of the fitted track with a detector element and the hit point read out by the detector element.

In the RHIC 2013 $p+p$ run, the PXL prototype detector took some low-luminosity data with stable configurations. Low-luminosity data are optimal for minimizing TPC space-charge distortions, tracking errors (mis-matches) and pileup effects. The total amount of data taken with the PXL detector together with the TPC is about 10 M events. Initial data quality assurance (QA) check was completed before carrying out the further alignment calibration. Hot channel masking was implemented based on the output sensor QA plots for removing hot channels from the calibration data. For sector global alignment, we used good TPC primary tracks fitted with the primary vertex. Tracks with transverse momentum $p_T \geq 1$ GeV/c with projections on the sensitive area of pixel were selected. Using primary tracks significantly improves precision of track projections on silicon detectors and reduces influence of systematics.

Figure 6 shows the residual distributions from single sector—sector 4 in ideal geometry before alignment. Residuals are shown in the TPC global coordinate system with Z direction along the beam direction and X–Y coordinate shown in Fig. 1.

Histogram-based alignment algorithm was proposed and applied in HFT PXL sector alignment. Alignment of PXL sector assumes that the sensor position on ladder and ladder position on the sector are frozen from survey data. The Jacobian equation below describes the algorithm for PXL detector alignment. The corresponding relations between track residuals and mis-alignments are described by 3 × 6 matrices. The transformation considers both shift and rotational mis-alignments and their cross talks. Six alignment parameters: 3 shift mis-alignments and 3 rotational mis-alignments, can be extracted from analyzing the plot of track residual as a function of the matrix elements.

We define mis-alignment of the detector in global coordinate system (GCS) as $\vec{\Delta} = (\Delta x, \Delta y, \Delta z, \Delta\alpha, \Delta\beta, \Delta\gamma)$ with six alignment parameters defined—shift mis-alignments in the X, Y, Z direction and rotational mis-alignments with respect to X, Y, Z-axes, respectively.

The Jacobian equation of measured hit position deviation from predicted ones with respect to mis-alignment parameters is in the form

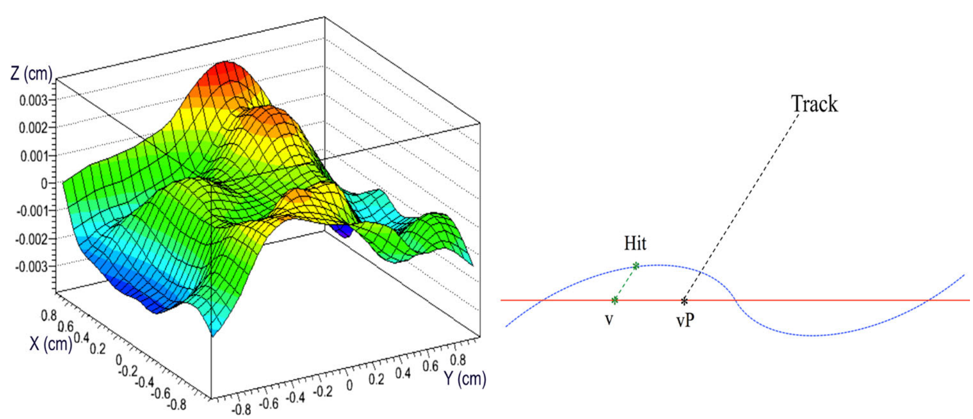

Fig. 5 (Color online) (*Left*) Sensor profile obtained from thin-plate spline. (*Right*) Hit–projection residual correction in the TPS plane

$$\vec{X_{\mathrm{hit}}} - \vec{X_{\mathrm{proj}}} = \partial\vec{X}/\partial\vec{\Delta}$$
$$= \vec{\Delta}\cdot\begin{pmatrix} -1+j_x v_x & j_x v_y & j_x v_z & j_x(-v_y z + v_z y) & -z + j_x(v_x z - v_z x) & y + j_x(-v_x y + v_y x) \\ j_y v_x & -1 + j_y v_y & j_y v_z & z + j_y(-v_y z + v_z y) & j_y(v_x z - v_z x) & -x + j_y(-v_x y + v_y x) \\ j_z v_x & j_z v_y & -1 + j_z v_z & -y + j_z(-v_y z + v_z y) & x + j_z(v_x z - v_y x) & j_z(-v_x y + v_y x) \end{pmatrix}, \quad (2)$$

where $\vec{j} = (j_x, j_y, j_z)$ is the track direction cosines in GCS on the measurement plane, $\vec{X} = (x, y, z)$ is the track projection in GCS on the measurement plane, $\vec{X_{\mathrm{hit}}} = (x_{\mathrm{hit}}, y_{\mathrm{hit}}, z_{\mathrm{hit}})$ is the hit position in GCS on measurement plane, and $\vec{v} = (v_x, v_y, v_z)$ is the direction perpendicular to the measurement plane in GCS.

The histogram-based method relies on the factorization of alignment steps. Mis-alignments can be extracted by calculating the slopes of the straight line fitted to the histograms of the most probable deviations versus the corresponding derivative matrix components. Practically, with slice fitting after minimizing background, the slope and intercept give rotational and shift mis-alignments through straight line fitting to the plot.

The alignment algorithm was extensively exercised with realistic simulation with an event generator and detector simulation package widely used in studies before applying to real data [19]. A series of blind tests were done with mis-alignments introduced in the geometry, and primary tracks from TPC alone were used as input. The algorithm was applied to the simulation data with geometry of sector arbitrarily shifted and rotated with good performance showing for track-based alignment.

Figure 7 shows an example of alignment of pixel individual sector—sector 4 with Y shift mis-alignment and γ rotation mis-alignment around the Z-axis (beam direction). The lines represent the results of linear fit with slope parameters corresponding to the measured mis-alignment (Δy or γ). Shown in the plots are the slopes measured before and after applying mis-alignment corrections. Black data points are mean values from slice fitting of the 2-D plots. The solid red lines depict a linear fit to the data points. The aligned results of sector 4 after three iterations of re-alignment are shown in the right two plots in the figure. We can see after correction, the shift and rotational mis-alignments were significantly pinned down to 40 microns and 0.06 mrad, respectively. One can obtain all six alignment parameters in the similar way. The quality of alignment has been estimated from residual distribution. It was found that histogram-based alignment method showed good performance and could tell the shifts or rotations to the precision in the order of tens of microns or a few mrad which meet our expectations.

In the RHIC 2014 run, full HFT detector alignment and inter-sector alignment were also done based on the same algorithm and procedures described above using cosmic ray data with much higher statistics. Histogram-based alignment check was also done for individual sector to confirm survey measurements as there are possible effects (temperature, air flow, etc.) that may potentially change the relative positions between detector elements during run period.

We notice that this track-based alignment algorithm is not sensitive to small mis-alignments in the order of few mrad or microns as it methodologically uses small angle approximation which could suffer from the cross talk between rotations and shifts. The issue may happen when a starting point is far from minimum because there are significant correlations among alignment parameters. Extensive studies were carried out, and it was found that multiple iteration does not further reduce mis-alignment and improve alignment performance. Interplay between shift and rotation is still under investigation. Sufficient statistics for good slice fitting are found essential for improving alignment precision. Further alignments using methods such as conventional residual minimization or hits and impact points (HIP) minimization method can provide further constraints on alignment parameters.

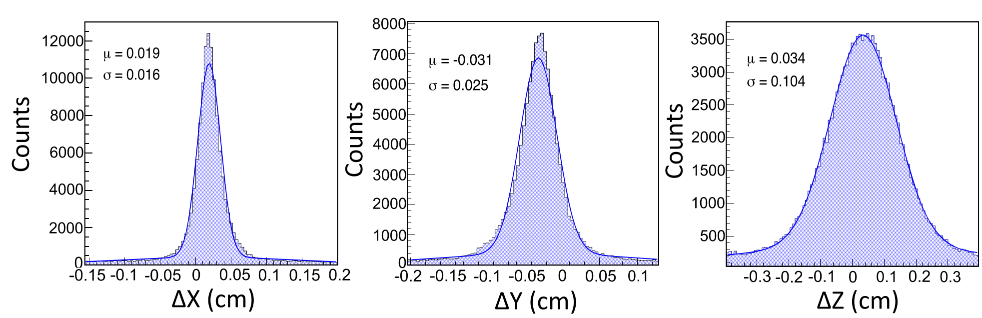

Fig. 6 (Color online) Residual distributions of PXL sector 4. Residual components in X, Y, Z directions in the STAR TPC global coordinate system are shown before alignment. TPC tracks projected on the PXL sensors with transverse momentum $p_{\mathrm{T}} \geq 1$ GeV/c were selected

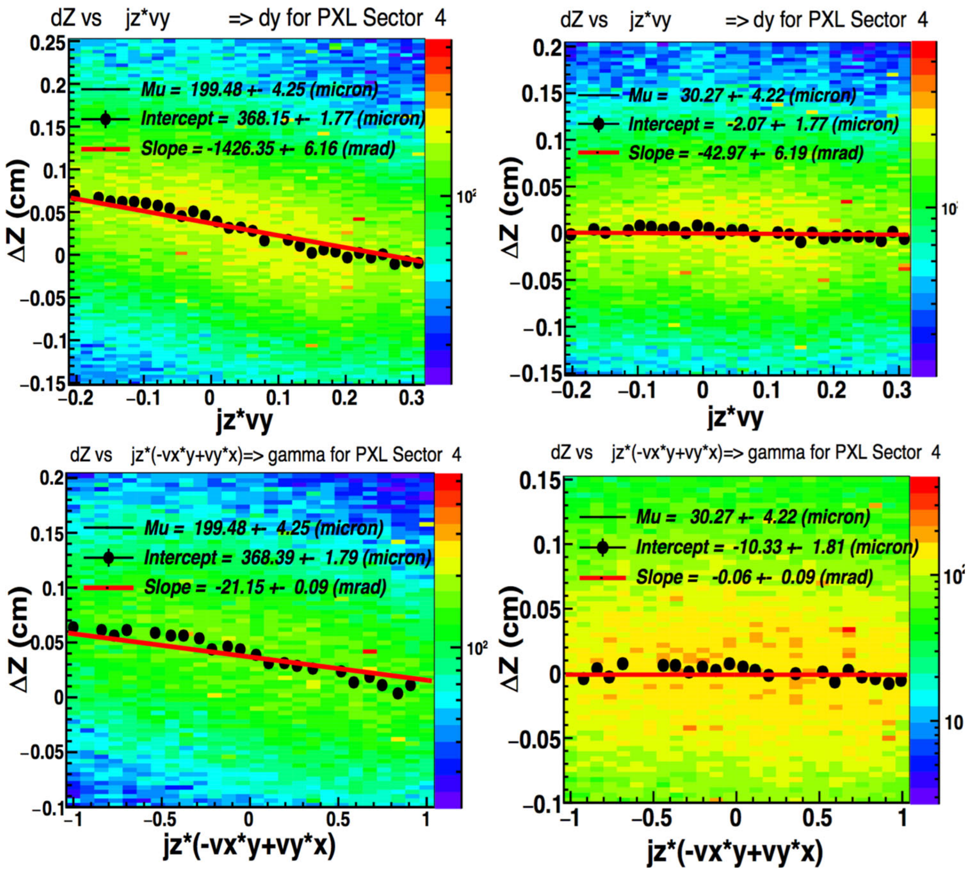

Fig. 7 (Color online) Global alignment calibration for PXL sector 4 using low-luminosity $p+p$ collision data from HFT engineering run with the histogram-based alignment method. Slope of the linear fitting gives the value of shift or rotational mis-alignment. (*Left plots*) Before alignment. (*Right plots*) After alignment

3.2 Performance study of the HFT PXL detector

We also studied the PXL detector performance in RHIC run 2013 and run 2014. Track going through overlapping active PXL areas allows a first estimation of intrinsic detector hit resolution. Collision data were used for the intrinsic hit resolution study. By taking the double residual of the tracks passing through the overlapping region of the sensors located quite close spatially, TPC tracking resolution can be greatly canceled out and PXL detector intrinsic hit resolution can be accessed.

Figure 8 shows the double residual distribution of PXL sector 4. The double residual is defined as the relative offset of hits and track projections between 2 overlapping sensors. Left plot shows result for tracks with $p_T > 1\,\text{GeV}/c$.

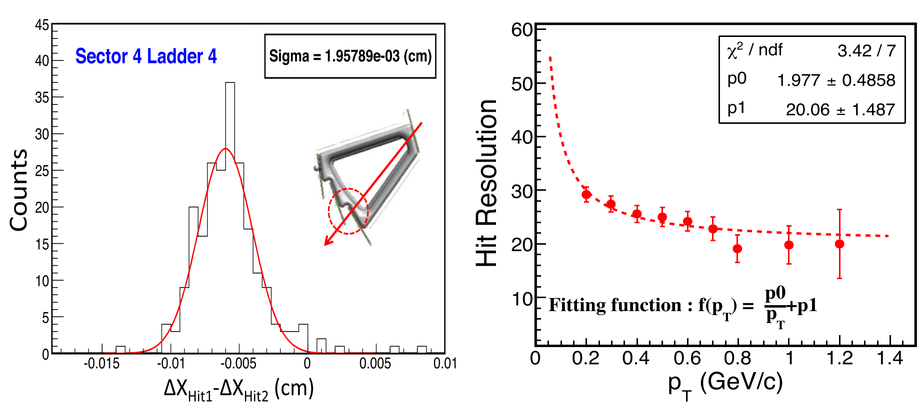

Fig. 8 (Color online) Double residual distribution of the tracks passing through overlapping regions in PXL sector 4 outer layer. (*Left plot*) Double residual distribution of tracks with p_T larger than 1 GeV/c. Embedded picture depicts track going through sensor overlapping region. (*Right plot*) Double residual resolution as a function of track transverse momentum. The hit resolution is in the unit of micrometer

The right plot of Fig. 8 shows the dependence of the spatial resolution along the global X direction as a function of the transverse momentum. The resulted single sensor resolution is around $19/\mathrm{sqrt}(2) = 13.4\,\mu\mathrm{m}$. Using tracks that pass through overlapping regions is also critical for survey measurement check or further aligning the offsets between ladders/sectors. In the HFT system, we have sufficient sensor overlapping region to make use of the double residual method for survey check or performance study.

In previous studies, the calibrations were all performed with the data collected with the magnetic field on. As STAR TPC tracking relies on the basic tracking procedures, TPC track resolution limits the performance study due to fake track–hit association resulting in uncontrolled residual background contribution. One way to minimize this impact is to run clean cosmic ray data. Cosmic ray traversing the STAR detector with large transverse momentum experiences little multiple scattering in the material providing an ideal tool to calibrate the detectors. The full system had been installed ahead of RHIC 2014 running to take zero-field cosmic data for performance study. Zero-field cosmic data obtained from runs during the January and February 2014 RHIC run were used for PXL efficiency study. The PXL discriminator thresholds were optimized according to the noise rates. Hot/dead pixels, columns and rows of PXL sensors were all flagged and masked out. Three clean hits on separate layers of sectors of PXL were selected out to define tracks and project outward to all PXL sensors for hit matching. Straight track reconstruction including all three hits without relying on STAR TPC tracking was done using zero-field cosmic ray data. Figure 9 shows the basic idea of cosmic ray track reconstruction with three PXL hits in separate layers.

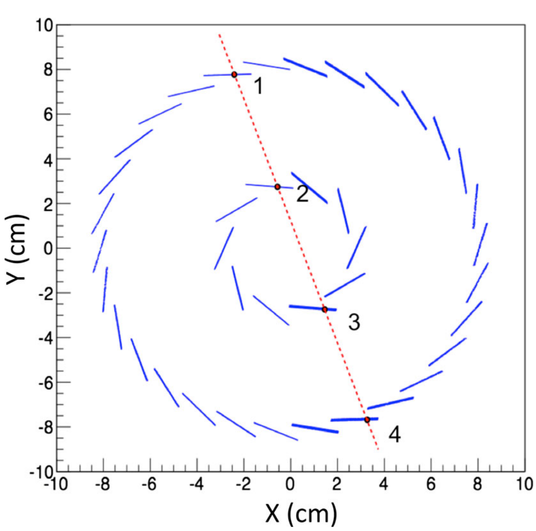

Fig. 9 (Color online) Two-dimensional display of zero-field cosmic ray track reconstruction with PXL hits. The straight-line cosmic ray reconstruction takes PXL hits 1, 2 and 3 and projects to PXL sensor with hit 4 associated. The track reconstruction requires at least one PXL hit in the inner layer and one PXL hit in the outer layer

The upper panel of Fig. 10 shows global X, Y and Z hit–projection residuals of whole PXL detector with track projections from normal TPC tracking. The lower panel shows the results after applying straight-line cosmic ray track reconstruction with PXL hits. The distribution indicates that the residual resolution after reconstruction was greatly improved and much closer to the PXL hit intrinsic resolution with significantly reduced background level.

The efficiency of the PXL detector was measured using cosmic ray tracks reconstructed from PXL hits with little mis-matching background contribution. The sensor efficiency is defined as

$$\text{Efficiency} = \frac{\text{Number of associated hits}}{\text{Number of projections}}, \tag{3}$$

where in the numerator, the number of projections is the total number of track projections on the sensor surface, and the denominator is the total number of associated readout hits with projections within 3σ residual resolution. Efficiency is measured for all the good sensors with hot/dead sensors excluded. The average PXL efficiency was measured to be 97.2% at the beginning of the RHIC 2014 run. The 2 gaps near sensor IDs 80 and 300 are due to the dearth of cosmic rays in the horizontal direction. The HFT subdetector IST efficiency was also measured in the similar way by outward projecting PXL tracks to the IST sensor sensitive area.

Detector performance optimization was done during the 14.5 GeV Au + Au run and early 200 GeV Au + Au run. The measurements shown in Fig. 11 were taken before detector optimization. Preliminary estimates on HFT performance after alignment are within physics design goals. Detector efficiency was tracked throughout the run. Several operational methods were developed and used during the run to minimize the efficiency loss due to radiative damage.

4 Conclusion

We present alignment calibration and performance study of the heavy flavor tracker PXL detector—the new silicon inner tracking detector installed for STAR experiment at RHIC. Track-based alignment algorithms developed for the HFT detector alignment were applied for alignment calibration within the HFT software framework. Large shift mis-alignments for PXL prototype sector 4 ($\Delta y \sim 600\,\mu\mathrm{m}$, $\Delta z \sim 300\,\mu\mathrm{m}$) and sector 7 ($\Delta x \sim 1100\,\mu\mathrm{m}$, $\Delta y \sim 300\,\mu\mathrm{m}$) were observed and corrected. Preliminary estimates on HFT PXL detector performance after alignment fulfilled physics and design goals. Further refinement can be

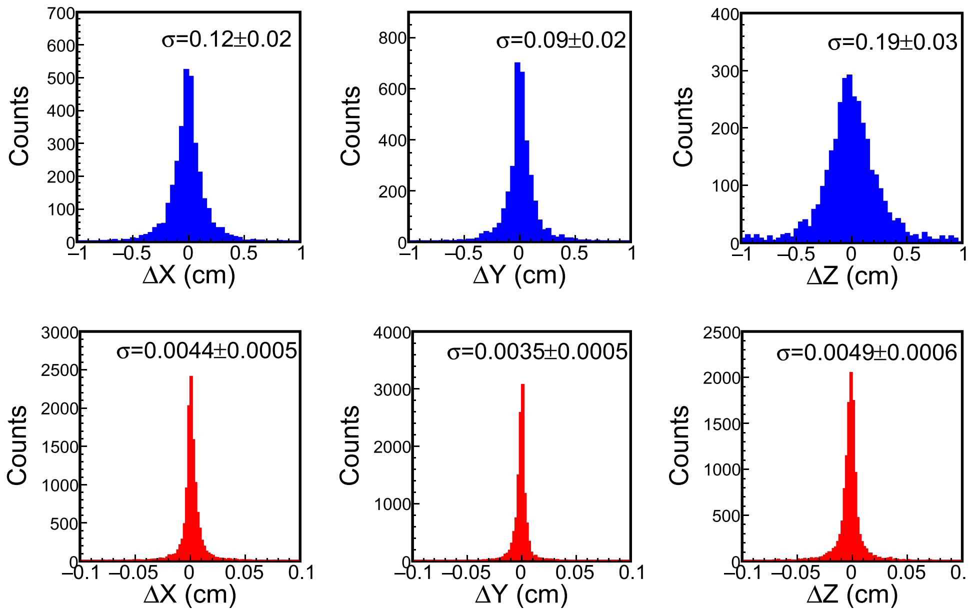

Fig. 10 (Color online) Hit–projection residual distributions in the global X, Y, Z directions for PXL detector. (*Upper panel*) Results from pure TPC tracking. (*Lower panel*) Results from straight-line cosmic ray track reconstruction based on PXL hit. The residual resolutions are shown in the *plots* for the zero-field cosmic ray data

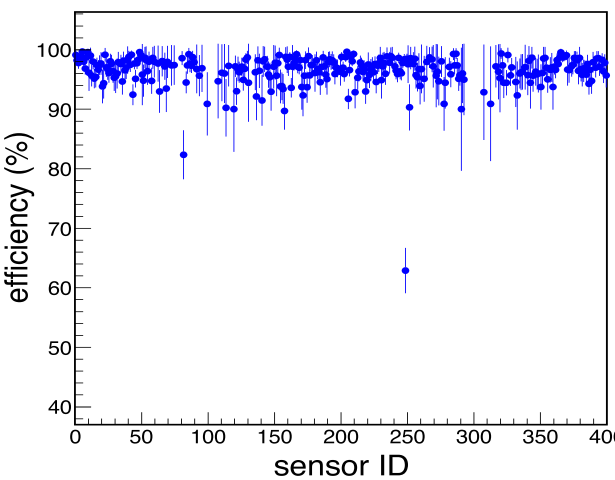

Fig. 11 (Color online) PXL sensor efficiency versus sensor ID

expected with detector performance optimization from the firmware side.

The intrinsic detector hit resolution of the HFT PXL detector was studied by looking into the double residuals of track projection–hit associations by taking advantage of the sensor overlapping regions. High intrinsic detector efficiency was observed showing good performance of the pixel sensors during run period. The heavy flavor tracker will enhance particle identification capability and enable precise open heavy flavor measurements at STAR by direct reconstructing displaced decay vertices. About 1200 M Au + Au 200 GeV minimum bias events were recorded with the PXL and IST detectors during the RHIC 2014 run. More collision data from the RHIC 2016 Au + Au run with HFT will come soon.

References

1. S.A. Chin, Transition to hot quark matter in relativistic heavy-ion collision. Phys. Lett. B **78**, 552 (1978). doi:10.1016/0370-2693(78)90637-8
2. J.I. Kapusta, Quantum chromodynamics at high temperature. Nucl. Phys. B **148**, 461 (1979). doi:10.1016/0550-3213(79)90146-9
3. F.M. Liu, Explore QCD phase transition with thermal photons. Nucl. Sci. Tech. **24**, 050524 (2013). doi:10.13538/j.1001-8042/nst.2013.05.024
4. H. Hahn, E. Forsyth, H. Foelsche et al., The RHIC design overview. Nucl. Instrum. Methods A **499**, 245–263 (2003). doi:10.1016/S0168-9002(02)01938-1
5. Z. Lin, M. Gyulassy, Nuclear gluon shadowing via continuum lepton pairs in $p + A$ at $\sqrt{s} = 200A$ GeV. Phys. Rev. Lett. **77**, 1222–1225 (1996). doi:10.1103/PhysRevLett.77.1222
6. Y. Zhang, J. Bouchet, X. Dong et al., Study of bottom production with the STAR Heavy Flavor Tracker. J. Phys. G Nucl. Part. Phys. **41**, 025103 (2014). doi:10.1088/0954-3899/41/2/025103
7. L. Adamczyk, G. Agakishiev, M.M. Aggarwal et al., (STAR), Measurements of D^0 and D^* production in $p + p$ collisions at $\sqrt{s} = 200$ GeV. Phys. Rev. D **86**, 072013 (2012). doi:10.1103/PhysRevD.86.072013
8. L. Adamczyk, J.K. Adkins, G. Agakishiev et al., (STAR), Observation of D^0 meson nuclear modifications in Au + Au collisions at $\sqrt{s_{\mathrm{NN}}} = 200$ GeV. Phys. Rev. Lett. **113**, 142301 (2014). doi:10.1103/PhysRevLett.113.142301
9. K.H. Ackermann, N. Adams, C. Adler et al., STAR detector overview. Nucl. Instrum. Methods A **499**, 624–632 (2003). doi:10.1016/S0168-9002(02)01960-5
10. HFT proposal, http://rnc.lbl.gov/wieman/hft-final-submission-version.pdf
11. D. Beavis et al., The STAR Heavy Flavor Tracker Technical Design Report, https://drupal.star.bnl.gov/STAR/starnotes/public/sn0600
12. W.J. Llope et al., Multigap RPCs in the STAR experiment at RHIC. Nucl. Instrum. Methods A **661**, S110–S113 (2012). doi:10.1016/j.nima.2010.07.086

13. M. Anderson, J. Berkovitz, W. Betts et al., The STAR time projection chamber: a unique tool for studying high multiplicity events at RHIC. Nucl. Instrum. Methods A **499**, 659–678 (2003). doi:10.1016/S0168-9002(02)01964-2
14. M. Beddo, E. Bielick, T. Fornek et al., The STAR barrel electromagnetic calorimeter. Nucl. Instrum. Methods A **499**, 725–739 (2003). doi:10.1016/S0168-9002(02)01970-8
15. STAR Collaboration, J. Adams, M.M. Aggarwal, Z. Ahammed et al., Pion, kaon, proton and anti-proton transverse momentum distributions from p + p and d + Au collisions at $\sqrt{s_{NN}} = 200$ GeV. Phys. Lett. B **616**, 8–16 (2005). doi:10.1016/j.physletb.2005.04.041
16. C. Hu-Guo, J. Baudot, G. Bertolone et al., First reticule size MAPS with digital output and integrated zero suppression for the EUDET-JRA1 beam telescope. Nucl. Instrum. Methods A **623**, 480–482 (2010). doi:10.1016/j.nima.2010.03.043
17. V. Karimaki et al., The HIP algorithm for track based alignment and its application to the CMS detector, CERN-CMS-NOTE-2006-018
18. V. Karimaki et al., Sensor alignment by traks—2003. Presented at CHEP. CMS CR-2004/009
19. X. Qin, R. Zhou, J.F. Han et al., GEANT4 simulation of the characteristic gamma-ray spectrum of TNT under soil induced by DT neutrons. Nucl. Sci. Tech. **26**, 010501 (2015). doi:10.13538/j.1001-8042/nst.26.010501